Nanocomposite formed by titanium ion implantation into alumina

R. E. Spirin, M. C. Salvadori, F. S. Teixeira, L. G. Sgubin, M. Cattani, and I. G. Brown

Citation: Journal of Applied Physics **116**, 184306 (2014); doi: 10.1063/1.4901643
View online: http://dx.doi.org/10.1063/1.4901643
View Table of Contents: http://scitation.aip.org/content/aip/journal/jap/116/18?ver=pdfcov
Published by the AIP Publishing

Nanocomposite formed by titanium ion implantation into alumina

R. E. Spirin,[1] M. C. Salvadori,[2,a)] F. S. Teixeira,[2] L. G. Sgubin,[2] M. Cattani,[2] and I. G. Brown[3]
[1]*Polytechnic School, University of São Paulo, Av. Prof. Luciano Gualberto 158, CEP 05508-970 São Paulo, SP, Brazil*
[2]*Institute of Physics, University of São Paulo, C.P. 66318, CEP 05314-970, São Paulo, SP, Brazil*
[3]*Lawrence Berkeley National Laboratory, Berkeley, California 94720, USA*

(Received 22 May 2014; accepted 2 November 2014; published online 13 November 2014)

Composites of titanium nanoparticles in alumina were formed by ion implantation of titanium into alumina, and the surface electrical conductivity measured *in situ* as the implantation proceeded, thus generating curves of sheet conductivity as a function of dose. The implanted titanium self-conglomerates into nanoparticles, and the spatial dimensions of the buried nanocomposite layer can thus be estimated from the implantation depth profile. Rutherford backscattering spectrometry was performed to measure the implantation depth profile, and was in good agreement with the calculated profile. Transmission electron microscopy of the titanium-implanted alumina was used for direct visualization of the nanoparticles formed. The measured conductivity of the buried layer is explained by percolation theory. We determine that the saturation dose, φ_0, the maximum implantation dose for which the nanocomposite material still remains a composite, is $\varphi_0 = 2.2 \times 10^{16}\,\mathrm{cm}^{-2}$, and the corresponding saturation conductivity is $\sigma_0 = 480\,\mathrm{S/m}$. The percolation dose φ_c, below which the nanocomposite still has basically the conductivity of the alumina matrix, was found to be $\varphi_c = 0.84 \times 10^{16}\,\mathrm{cm}^{-2}$. The experimental results are discussed and compared with a percolation theory model. © *2014 AIP Publishing LLC*.
[http://dx.doi.org/10.1063/1.4901643]

I. INTRODUCTION

Nanocomposites composed of metal nanoparticles in an insulating matrix can be fabricated by metal ion implantation,[1–11] thereby forming a buried layer whose electrical conductivity can be tailored by control of the implantation dose. The electrical conductivity of the nanocomposite layer has been described mathematically by a number of theories of electron transport in isotropic percolating materials.[12] We have studied the electrical characteristics of the buried layer formed by titanium ion implantation into alumina. Alumina insulators whose surface has been modified in this way are especially important for fabricating high-voltage insulators with controlled surface resistivity, and metal ion implantation into alumina has been used for this purpose.[13–18] High voltage accelerator columns have been prepared in this way,[14–16] and support rods for electrostatic focusing lenses in single-ion devices.[18] In these applications, the objective is to bleed off surface charge accumulation while maintaining an uniform voltage gradient across the insulator surface, avoiding surface breakdown and maximizing the voltage-hold-off capability of the component. Although this approach has been used with considerable success, theoretical understanding of the processes involved is still not completely established.

In prior work, we have studied a number of nanocomposites formed by ion implantation, including Au/PMMA (polymethylmethacrylate),[1–8] Pt/PMMA,[9] and Au/alumina.[11] Some of our experiments have included Ti/alumina[10] nanocomposites, and the results of these prior investigations are discussed in the present work. The Ti/alumina samples were formed using titanium ion implantation, and *in situ* conductivity measurements were performed as the implantation proceeded, thus providing data of the surface electrical conductivity as a function of the implantation dose. To assist in analysis and interpretation of the results, the TRIDYN computer code[19,20] was used to estimate the depth profiles of the ion implanted titanium in the alumina substrate. Rutherford backscattering spectrometry (RBS) was performed to confirm the TRIDYN simulation results, and transmission electron microscopy (TEM) of the titanium-implanted alumina was used for direct visualization of the nanoparticles formed.

II. THEORETICAL BACKGROUND

We have reviewed in prior work[21] the theoretical understanding and experimental results about the electrical characteristics of nanocomposites formed by metal nanoparticles embedded in an insulating matrix. Here, we briefly summarize. The electrical conductivity σ of nanocomposite materials, near the critical conductor-insulator transition, is given by the scaling law

$$\sigma \approx \sigma_0 (x - x_c)^t, \tag{1}$$

where σ_0 is a proportionality constant equal to the saturation conductivity, for which the material still remains a composite, x is the *normalized metal atom concentration* of the conducting phase, x_c is the *critical concentration*, or *percolation threshold*, below which the composite has the same conductivity as the insulating host matrix, and t is the *critical*

a)Author to whom correspondence should be addressed. Electronic mail: mcsalvadori@if.usp.br

exponent. For nanocomposites formed by metal ion implantation into an insulating substrate, we define the normalized metal atom concentration x by the ratio φ/φ_0, where φ is the ion dose implanted and φ_0 is the *saturation dose*, that is, the maximum dose for which the material still remains a composite; for doses greater than φ_0 ($x=\varphi/\varphi_0>1$), a metal film starts to be deposited on the insulator surface and the material begins to take on the characteristics of a thin metal film. The electron transport through nanocomposites formed in this way can occur through either of two processes or their combination. When the conducting nanoparticles are in geometric contact, the process is called *percolation* and the theoretical prediction is that the critical exponent t is less than 2.[12] When the system is *percolated*, electrically it can be viewed as a random resistor network. When the conducting nanoparticles are not in geometric contact, an inter-particle tunneling process is dominant. Both processes—percolation and tunneling—may contribute, and in this case, the theoretical prediction[12] is that the critical exponent t is greater than two and the process is called *tunneling-percolation*. Note that in this kind of material we can distinguish three different regimes: (1) *conductor* ($x>x_c$), (2) *transition* ($x\approx x_c$), and (3) *insulator* ($x<x_c$).

Nanocomposite formation is a random process and Monte Carlo calculations form the mathematical basis used to study percolation and the electrical transport processes. Kirkpatrick[22] developed an "effective medium theory," in which the system is considered as a random resistor network. According to Kirkpatrick the effective conductivity of the nanocomposite is given by

$$\frac{\sigma}{\sigma_1}=\frac{\left(z\frac{x}{2}-1\right)+\left(z\frac{(1-x)}{2}-1\right)\frac{\sigma_2}{\sigma_1}+\left\{\left[\left(z\frac{x}{2}-1\right)+\left(z\frac{(1-x)}{2}-1\right)\frac{\sigma_2}{\sigma_1}\right]^2+2(z-2)\frac{\sigma_2}{\sigma_1}\right\}^{\frac{1}{2}}}{z-2}, \tag{2}$$

where z is the number of bonds at each node of the network, σ_1 is the conductivity of the conducting phase, σ_2 is the conductivity of the insulating phase, and x is the normalized metal atom concentration. Using this expression, one can calculate analytically the effective conductivity σ/σ_1. The σ/σ_1 values calculated from this equation, though based on resistor-network theory, are accurate[22,23] and in good agreement with numerical Monte Carlo calculations.

III. EXPERIMENTAL

The samples were prepared by ion implanting titanium into alumina substrates. The implantation system used in this work is in essence a vacuum arc ion source-based implantation facility,[24] but in modified form that allows a much simplified and physically smaller arrangement. The equipment used for the ion implantation has been described in detail in the literature.[25,26] In this technique, the ion source and the plasma are held at ground potential, while the final grid and the substrate are held at high negative potential. The extractor voltage used was 25 kV. The titanium plasma (formed by a vacuum arc discharge) from which the ion beam is formed is composed of multiply charged ion species, and for titanium the charge state distribution is known[24] to be Ti^+: Ti^{2+}: $Ti^{3+}=11:75:14$ (particle percent), corresponding to a mean charge state $Q=2.1$. Thus, the mean ion implantation energy was 52.5 keV. The implantation is done in a repetitively pulsed mode[25,26] with 100 μs pulses at a repetition rate of 3 Hz. A magnetically suppressed Faraday cup at the target location monitors the beam current, which was about 11 mA/cm^2 peak pulsed, or a time-averaged ion implantation current density of about 3.3 μA/cm^2.

Two alumina substrates, each of the same size, were prepared with electrical contacts at both ends of the alumina substrate. The electrical contacts were formed by ceramic-to-metal welding.[27] Two independent and identical experiments were carried out using both substrates thus prepared, generating sample 1 and sample 2. The substrate was positioned at the entrance to the Faraday cup, but not completely covering it and thus allowing the dose to be monitored. As the implantation proceeded, the conductivity measurements were performed *in situ*. After a certain number of pulses of known dose (measured by the Faraday cup), the implantation process was temporarily suspended and the sample resistance measured, after which the implantation proceeded, and so on, generating data of resistance as a function of dose. The conductivity, σ, for each implantation dose was obtained considering the dimensions of the region, where the nanocomposite was formed in the substrate. For this purpose, we used the following equation:

$$\sigma=\ell/Rwd, \tag{3}$$

where R is the measured resistance, ℓ is the length of the region over which the nanocomposite was formed, w is the width of this region, and d is the thickness of the nanocomposite layer. A photograph of one of the samples, showing

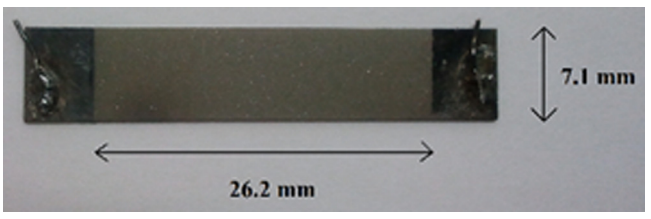

FIG. 1. Photograph of alumina sample after implantation with titanium, showing the electrical contacts formed by ceramic-to-metal welding. The area implanted is (26.2×7.1) mm^2.

the region where the nanocomposite was formed, is shown in Figure 1, where $\ell = 26.2$ mm and $w = 7.1$ mm. The nanocomposite layer thickness, d, was estimated by TRIDYN numerical simulation as described below.

The depth profiles expected for titanium-implanted alumina were calculated using TRIDYN.[19,20] This computer code uses a Monte Carlo simulation program based on the TRIM (Transport and Range of Ions in Matter) code.[28] TRIDYN includes two additional factors: change in the substrate composition as the implantation proceeds, and sputtering (erosion) of the substrate surface. The TRIDYN program should be used when the implantation dose is moderate-to-high, since the composition of the substrate changes significantly during the implantation process and significant sputtering may occur.

RBS analysis was also carried out to measure the Ti depth profile so as to provide a comparison and confirmation of the TRIDYN calculation. The RBS was done on an alumina sample that had been Ti-implanted to a dose $1 \times 10^{16}\,\mathrm{cm}^{-2}$ (and at 52.5 keV)

TEM was performed to visualize the titanium nanoparticles inside the alumina substrate. For sample preparation, an alumina plate was scratched with a diamond tip to obtain alumina powder. The powder was sifted with a sieve of mesh size 0.062 mm for removing large grains. The powder was placed on a piece of lens cleaning paper, scrubbed, and the excess removed, leaving on the surface alumina particles with grain size small enough for TEM observation. Titanium implantation was then carried out into the alumina powder-on-paper sample, using the same parameters as described above. Finally, a TEM copper grid coated with thin films of formvar and carbon was moistened in deionized water and rubbed on the implanted powder-on-paper, yielding a useable TEM sample. The transmission electron microscope used was a Jeol model JEM-2100. The samples thus prepared were observed before and after titanium ion implantation. Energy-dispersive X-ray Spectroscopy (EDS) confirmed the titanium content of each nanoparticle.

The method we used for determining the saturation dose (φ_0) and the saturation conductivity (σ_0), for which the Ti-implanted alumina still remains a composite, is described in the Appendix.

IV. RESULTS AND DISCUSSION

Figure 2 shows the results of TRIDYN computer simulations of the titanium depth profile in the alumina substrate. The titanium atomic fraction is plotted as a function of depth below the substrate surface (i.e., the alumina surface is located at zero depth). The different curves refer to doses between $0.5 \times 10^{16}\,\mathrm{cm}^{-2}$ and $3 \times 10^{16}\,\mathrm{cm}^{-2}$ for implantation at an energy of 52.5 keV. The depth of the maximum Ti concentration depends on the dose, and decreases with increasing dose, being between 25 nm (for the highest dose) and 29 nm (for the lowest dose). This behavior is expected since previously implanted material works as a kind of barrier to subsequently implanted material, causing the implanted material to increasingly accumulate closer to the surface; in addition, sputtering of the surface during implantation reduces the thickness of the substrate material above the

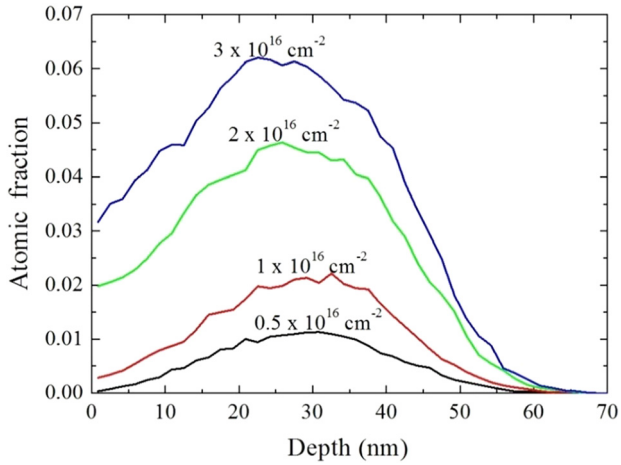

FIG. 2. TRIDYN simulations of the titanium atomic fraction as a function of depth; the alumina surface is at zero depth. The different curves refer to doses from $0.5 \times 10^{16}\,\mathrm{cm}^{-2}$ to $3 \times 10^{16}\,\mathrm{cm}^{-2}$, for titanium implantation into alumina at 52.5 keV.

composite layer. The thickness of the nanocomposite layer (d) was evaluated as the depth range for which the Ti concentration was greater than 10% of the maximum, for each dose simulated. The d value was about 55 nm for all doses.

Figure 3 shows the depth profile of Ti implanted into alumina at a dose of $1 \times 10^{16}\,\mathrm{cm}^{-2}$ and mean ion energy 52.5 keV (extraction voltage 25 kV), as determined by RBS measurement and by TRIDYN computer simulation. Clearly, the agreement between measurement and calculation is good with respect to depth of the buried layer and atomic concentration. The RBS-measured width of the profile is, however, somewhat broader than the simulation. We ascribe this as being due to the Ti ion beam having a charge state structure that is not included in the TRIDYN simulation. As described above, the beam has a charge state distribution as Ti^{+}: Ti^{2+}: $Ti^{3+} = 11{:}75{:}14$ (particle percent), and thus for an extraction voltage of 25 kV an ion energy structure in which 11% of the beam ions are of energy 25 keV, 75% at 50 keV, and 14% at 75 keV, leading to a somewhat broader implantation depth profile than calculated for a mono-energetic beam at a mean

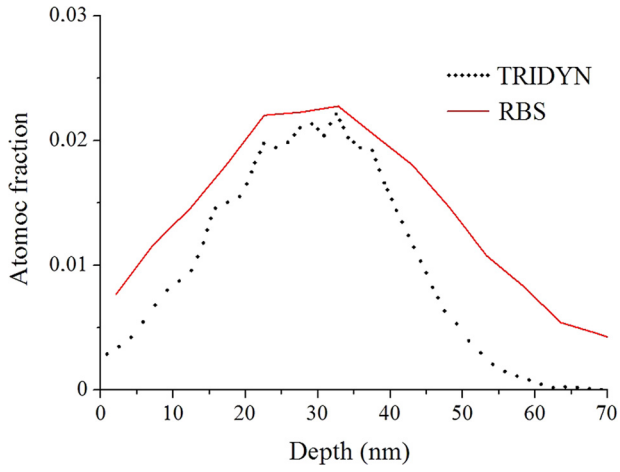

FIG. 3. Depth profile of Ti implanted into alumina at a dose of $1 \times 10^{16}\,\mathrm{cm}^{-2}$ and mean ion energy 52.5 keV (extraction voltage 25 kV), as determined by RBS measurement and by TRIDYN computer simulation.

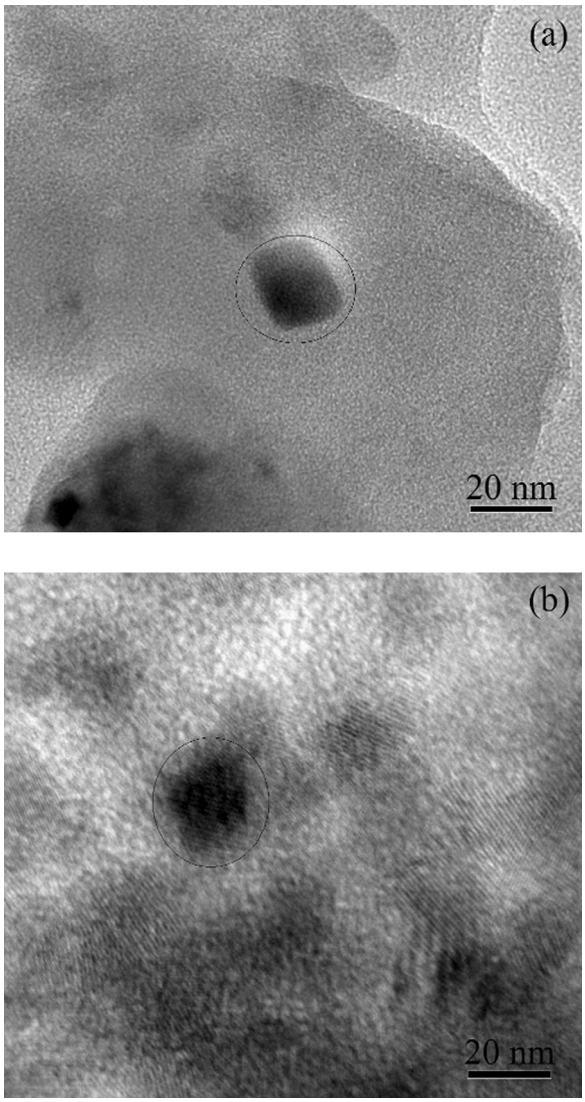

FIG. 4. Typical TEM micrographs of Ti-implanted alumina with ion energy 52.5 keV. (a) Implantation dose $0.6 \times 10^{16}\,\mathrm{cm}^{-2}$ and (b) implantation dose $1 \times 10^{16}\,\mathrm{cm}^{-2}$. The circles identify the Ti nanoparticles, confirmed by EDS analysis.

energy of 52.5 keV. Nevertheless, the effect is small and of minor consequence to the present work.

It is known[29] that metal nanoparticles nucleate and grow when the metal atom concentration implanted into the substrate (matrix material) exceeds the solubility limit. The TEM results obtained here support the idea of titanium nanoparticle formation. Ti ion implantation was performed with ion energy of 52.5 keV and two samples with different doses were prepared: $0.6 \times 10^{16}\,\mathrm{cm}^{-2}$ and $1 \times 10^{16}\,\mathrm{cm}^{-2}$. Typical TEM micrographs of the Ti-implanted alumina are shown in Figure 4, where one can see titanium nanoparticles (encircled as a guide to the eye). EDS analysis confirmed the titanium content of each nanoparticle. The average size of the nanoparticles is about 20 nm.

Thus, we infer that titanium nanoparticles nucleate first at the depth at which the atomic fraction is maximum,[29] at a depth of between 25 and 29 nm below the alumina surface. We also hypothesize that the nanocomposite layer formed below the alumina surface will be close to a bi-dimensional

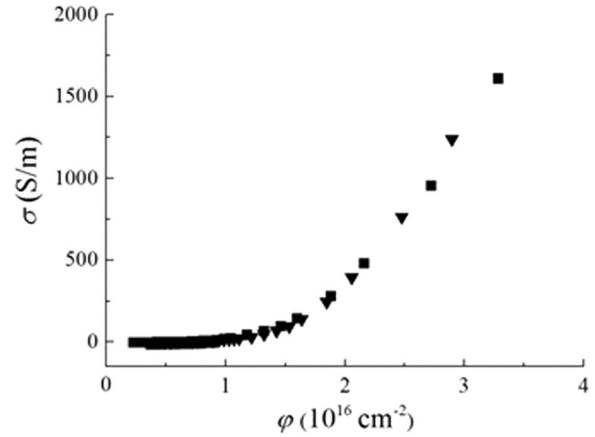

FIG. 5. Measured conductivity, σ, as a function of Ti dose, φ, implanted into alumina. The data points shown as squares and triangles correspond to results from two independent experiments (samples 1 and 2, respectively).

layer, limiting the number of nearest neighbors for each titanium nanoparticle to between $z = 5$ and $z = 6$. Thus, finally, we estimate the thickness, d, of the nanocomposite layer as being 55 nm (see Figure 2), and this we use for the conductivity calculation of Eq. (3).

Plots of the measured conductivity, σ, as a function of the implanted dose, φ, are shown for samples 1 and 2 in Figure 5. These results were generated through two independent and identical experiments, indicating the excellent reproducibility of the results. With these data and guided by the theoretical predictions of Eqs. (1) and (2), we estimate (see the Appendix of this work) the saturation conductivity, σ_0, and the saturation dose, φ_0, as $\sigma_0 = 480\,\mathrm{S/m}$ and $\varphi_0 = 2.2 \times 10^{16}\,\mathrm{cm}^{-2}$.

Figure 6 shows the normalized conductivity, σ/σ_0, as a function of the normalized implantation dose, $x = \varphi/\varphi_0$, for samples 1 and 2. As explained in the Appendix, the percolation dose, φ_c, below which the nanocomposite still has basically the conductivity of the alumina matrix, and the critical exponent, t, are determined together with the saturation conductivity, σ_0, and the saturation dose, φ_0. They were found to be $\varphi_c = 0.84 \times 10^{16}\,\mathrm{cm}^{-2}$, corresponding to $x_c = 0.38$ and $t = 1.4$. Since the critical exponent obeys the condition

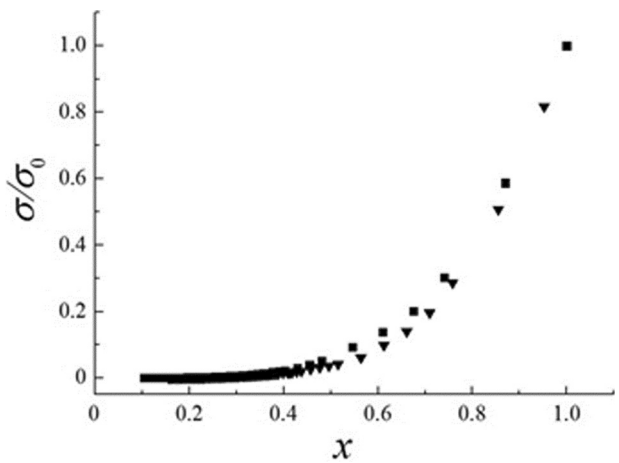

FIG. 6. Normalized conductivity, σ/σ_0, as a function of the normalized implanted dose, $x = \varphi/\varphi_0$, for samples 1 (squares) and 2 (triangles).

$t < 2.0$, we conclude that the conductivity process is due to percolation, with the contribution from tunneling conduction being negligible.[12]

In prior work,[10] we prepared four similar samples, with titanium implanted into alumina at an energy of 75 keV and doses of 0.63×10^{16}, 1.89×10^{16}, 3.00×10^{16}, and $6.05 \times 10^{16}\,\mathrm{cm}^{-2}$, and measured the sheet resistance. The results were analyzed using a similar approach to that used in the present work, considering the formation of an insulator-conductor composite of alumina and nanoparticles of partially oxidized titanium. The results obtained showed that the normalized percolation dose, $x_c = \varphi_c/\varphi_0$, was within the interval of 0.31–0.5, which is quite consistent with results of the present work ($x_c = 0.38$) as described above. The saturation conductivity was between 14 and 3000 S/m, which is within the acceptable range for partially oxidized titanium,[30] and it is compatible with the results of the present work ($\sigma_0 = 480$ S/m). However, the saturation dose, φ_0, was estimated[10] to be between 6×10^{16} and $20 \times 10^{16}\,\mathrm{cm}^{-2}$, compared to the lower value of $\varphi_0 = 2.2 \times 10^{16}\,\mathrm{cm}^{-2}$ obtained in the present work; and similarly, the percolation dose, φ_c, was estimated to be between 3×10^{16} and 6×10^{16} cm^2, compared to the lower value of $\varphi_c = 0.84 \times 10^{16}\,\mathrm{cm}^{-2}$ obtained in the present work. We surmise that the origin of the lower values for saturation dose and percolation dose found in the present work is that the equipment used for the titanium implantation in the prior work was not the same as that used in the present work, and could well have led to a higher level of oxygen incorporation than in the present work.

To explore the possibility of long-term increased oxidation of the buried titanium nanoparticles, we monitored the resistance of the samples for a period of about 80 days after removal from the implantation chamber. We found a resistance increase of about 1% for one of the samples and about 2% for the other, showing that the long-term oxidation of nanoparticles below the alumina surface is minimal.

V. SUMMARY AND CONCLUSION

Nanocomposites obtained by titanium ion implantation into alumina were characterized *in situ* by measuring the sheet resistance (resistivity of the buried nanocomposite layer) as the implantation proceeded. The ion implantation energy used was 52.5 keV. The computer code TRIDYN was used to estimate the depth profiles of the implanted titanium. The depth of the maximum implanted titanium concentration is the expected location of the titanium nanoparticle layer, and the TRIDYN results showed that this depth depends on the dose and decreases with increasing dose. The maximum titanium atomic fraction lay between 25 nm (for the highest dose simulated, $3 \times 10^{16}\,\mathrm{cm}^{-2}$) and 29 nm (for the lowest dose simulated, $0.5 \times 10^{16}\,\mathrm{cm}^{-2}$) below the alumina surface. The nanocomposite layer thickness, d, was estimated as being 55 nm. RBS measurement of the Ti depth profile was in good agreement with the TRIDYN simulation results, except for the buried layer width being somewhat broader than calculated, a consequence of the Ti ion charge state structure and hence ion beam energy structure. TEM images confirm titanium nanoparticle formation, with average size about 20 nm. EDS analysis confirmed the titanium content of the nanoparticles visualized by TEM. The resistivity results indicate a saturation conductivity of $\sigma_0 = 480$ S/m and a saturation dose of $\varphi_0 = 2.2 \times 10^{16}\,\mathrm{cm}^{-2}$. The percolation dose, $\varphi_{c,}$ was found to be $\varphi_c = 0.84 \times 10^{16}\,\mathrm{cm}^{-2}$, corresponding to $x_c = \varphi_c/\varphi_0 = 0.38$, obtained using a theory in which the system is considered as a random resistor network. The critical exponent obtained was $t = 1.4$, and since this value satisfies the condition $t < 2.0$, we conclude that the conductivity process is due to percolation, with the contribution from tunneling conduction being negligible. We also confirmed that the buried titanium nanoparticles did not continue to oxidize to any significant extent after exposure to ambient conditions; the samples displayed a resistance increase of between 1% and 2% after 80 days in our laboratory atmosphere.

ACKNOWLEDGMENTS

This work was supported by the Fundação de Amparo a Pesquisa do Estado de São Paulo (FAPESP) and the Conselho Nacional de Desenvolvimento Científico e Tecnológico (CNPq), Brazil. We are grateful to the Institute of Ion Beam Physics and Materials Research at the Forschungszentrum Dresden-Rossendorf, Germany, for the TRIDYN-FZR computer simulation code.

APPENDIX: DETERMINATION OF SATURATION DOSE AND CONDUCTIVITY

In this work, we used Eq. (1) and the Kirkpatrick predictions, given by Eq. (2) (using $\sigma_1 = 2.4 \times 10^6$ S/m and $\sigma_2 = 1 \times 10^{-12}$ S/m), for estimating the saturation dose, φ_0, the saturation conductivity, σ_0, for which the Ti-implanted alumina still remains a composite, the normalized percolation dose, $x_c = \varphi_c/\varphi_0$, and the critical exponent, t. For this purpose, we substitute $x = \varphi/\varphi_0$ and $x_c = \varphi_c/\varphi_0$ in Eq. (1), where φ_c is the percolation dose, and differentiate with respect to φ, to obtain

$$\frac{d\sigma}{d\varphi} = \frac{\sigma_0 t}{\varphi_0}\left(\frac{\varphi}{\varphi_0} - \frac{\varphi_c}{\varphi_0}\right)^{(t-1)} \tag{A1}$$

which can be expressed (taking the logarithm) as

$$\ln\left(\frac{d\sigma}{d\varphi}\right) = \ln\left(\frac{\sigma_0 t}{\varphi_0}\right) + (t-1)\ln\left(\frac{\varphi}{\varphi_0} - \frac{\varphi_c}{\varphi_0}\right). \tag{A2}$$

Equation (A2) can be seen as a linear equation of the form

$$Y = C + \alpha X, \tag{A3}$$

where $Y = \ln\left(\frac{d\sigma}{d\varphi}\right)$, $C = \ln\left(\frac{\sigma_0 t}{\varphi_0}\right)$, $\alpha = (t-1)$, and $X = \ln\left(\frac{\varphi}{\varphi_0} - \frac{\varphi_c}{\varphi_0}\right)$, and where σ and φ are experimental values, and σ_0, φ_0, φ_c, and t are to be determined. To solve this, we take the experimental σ^* values as a function of φ^* and the predicted values for $x_c = \varphi_c/\varphi_0$ (estimated from Eq. (2), considering z between 5 and 6) and fit Eq. (A3) for different pairs (σ_0^*, φ_0^*) from the experimental data. For each fit, we can verify the self-consistency of the result by taking the t

and C values obtained from the fit and calculating $\ln\left(\frac{\sigma_0^* t}{\varphi_0^*}\right)$. When C attains the same value as $\ln\left(\frac{\sigma_0^* t}{\varphi_0^*}\right)$, then the pair ($\sigma_0$*, φ_0*) is the correct saturation conductivity and saturation dose, respectively, and t is also determined.

[1]M. C. Salvadori, M. Cattani, F. S. Teixeira, and I. G. Brown, Appl. Phys. Lett. **93**, 073102 (2008).
[2]F. S. Teixeira, M. C. Salvadori, M. Cattani, S. M. Carneiro, and I. G. Brown, J. Vac. Sci. Technol., B **27**, 2242 (2009).
[3]F. S. Teixeira, M. C. Salvadori, M. Cattani, and I. G. Brown, J. Appl. Phys. **106**, 056106 (2009).
[4]F. S. Teixeira, M. C. Salvadori, M. Cattani, and I. G. Brown, J. Appl. Phys. **105**, 064313 (2009).
[5]F. S. Teixeira, M. C. Salvadori, M. Cattani, and I. G. Brown, J. Appl. Phys. **108**, 093505 (2010).
[6]F. S. Teixeira, M. C. Salvadori, M. Cattani, and I. G. Brown, J. Vac. Sci. Technol., A **28**, 818 (2010).
[7]F. S. Teixeira, M. C. Salvadori, M. Cattani, and I. G. Brown, J. Appl. Phys. **111**, 104311 (2012).
[8]J. Ferreira, F. S. Teixeira, A. R. Zanatta, M. C. Salvadori, R. Gordon, and O. N. Oliveira, Jr., Phys. Chem. Chem. Phys. **14**, 2050 (2012).
[9]M. C. Salvadori, F. S. Teixeira, M. Cattani, and I. G. Brown, J. Appl. Phys. **110**, 114905 (2011).
[10]M. C. Salvadori, F. S. Teixeira, M. Cattani, A. Nikolaev, K. P. Savkin, E. M. Oks, H.-K. Park, L. Phillips, K. M. Yu, and I. G. Brown, J. Appl. Phys. **111**, 063714 (2012).
[11]M. C. Salvadori, F. S. Teixeira, L. G. Sgubin, M. Cattani, and I. G. Brown, Nucl. Instrum. Methods Phys. Res., Sect. B **310**, 32 (2013).
[12]S. Vionnet-Menot, C. Grimaldi, T. Maeder, S. Strässler, and P. Ryser, Phys. Rev. B **71**, 064201 (2005).
[13]C. W. White, C. J. McHargue, P. S. Sklad, L. A. Boatner, and G. C. Farlow, Mater. Sci. Rep. **4**, 41 (1989).
[14]S. Anders, A. Anders, and I. Brown, in IEEE 1993 Particle Accelerator Conference, Washington, D.C., 17–20 May 1993, edited by C. W. Leemann and J. J. Bisognano (IEEE, 1994).
[15]F. Liu, I. Brown, L. Phillips, G. Biallas, and T. Siggins, in *Proceedings of 1997 IEEE Particle Accelerator Conference, Vancouver, B.C. Canada*, 12–16 May 1997 (1997), Vol. 3, pp. 3752–3754.
[16]F. Liu, M. R. Dickinson, R. A. MacGill, A. Anders, O. R. Monteiro, I. G. Brown, L. Phillips, G. Biallis, and T. Siggins, Surf. Coat. Technol. **103/104**, 46 (1998).
[17]D. Li, J. Zhang, M. Yu, J. Kang, and W. Li, Appl. Surf. Sci. **252**, 1029 (2005).
[18]A. Nikolaev, E. M. Oks, K. Savkin, G. Yu. Yushkov, D. J. Brenner, G. Johnson, G. Randers-Pehrson, I. G. Brown, and R. A. MacGill, Surf. Coat. Technol. **201**, 8120 (2007).
[19]W. Möller and W. Eckstein, Nucl. Instrum. Methods Phys. Res., Sect. B **2**, 814 (1984).
[20]W. Möller, W. Eckstein, and J. P. Biersack, Comput. Phys. Commun. **51**, 355 (1988).
[21]M. Cattani, M. C. Salvadori, and F. S. Teixeira, Insulator-Conductor Transition: a Brief Theoretical Review, see http://arxiv.org/ftp/arxiv/papers/0903/0903.3587.pdf.
[22]S. Kirkpatrick, Phys. Rev. Lett. **27**, 1722 (1971).
[23]S. Kirkpatrick, Rev. Mod. Phys. **45**, 574 (1973).
[24]E. M. Oks and I. G. Brown, in *The Physics and Technology of Ion Sources*, edited by Ian Brown (Wiley-VCH, Weinheim, 2004), pp. 257–284.
[25]M. C. Salvadori, F. S. Teixeira, L. G. Sgubin, W. W. R. Araujo, R. E. Spirin, E. M. Oks, K. M. Yu, and I. G. Brown, Appl. Phys. Lett. **101**, 224104 (2012).
[26]M. C. Salvadori, F. S. Teixeira, L. G. Sgubin, W. W. R. Araujo, R. E. Spirin, E. M. Oks, and I. G. Brown, Rev. Sci. Instrum. **84**, 023506 (2013).
[27]H. J. de Bruin, A. F. Moodie, and C. E. Warble, J. Mater. Sci. **7**, 909 (1972).
[28]J. F. Ziegler, J. P. Biersack, and U. Littmark, *The Stopping and Range of Ions in Solids* (Pergamon, New York, 1985 (new edition in 1996)). The computer code is downloadable from the SRIM website http://www.srim.org/.
[29]A. L. Stepanov, D. E. Hole, and P. D. Townsend, J. Non-Cryst. Solids **260**, 65 (1999).
[30]K. W. Vogt, P. A. Kohl, W. B. Carter, R. A. Bell, and L. A. Bottomley, Surf. Sci. **301**, 203 (1994).